Journal of Petroleum Research and Studies

Open Access
No. 34 part 1, March 2022, pp.154-172

P- ISSN: 2220-5381
E- ISSN: 2710-1096

DOI: http://doi.org/10.52716/jprs.v12i1.596

Numerical Study of Oil-water Separation in Inline Axial Hydrocyclone

Karima E. Amori*, Zainab H. Al-Ammar
Department of Mechanical Engineering, College of Engineering, University of Baghdad, Baghdad, Iraq.
*Corresponding Author E-mail: drkarimaa63@gmail.com

6th Iraq Oil and Gas Conference, 29-30/11/2021

Abstract

The fluid mixture hydrocyclone is an excellent tool for downhole oil/water separation (DOWS) for high water cut. In the present work the flow through inline axial inlet hydrocyclone is investigated computationally using ANSYS-FLUENT-19 software. The three dimensional continuity and momentum equations with SST k-omega turbulence model are used to simulate the strongly swirling, turbulent flow. Oil/water two phase mixture treated as the working fluid, water is considered as the primary phase and oil is the secondary phase. The considered oil volume fraction this work is 0.25 and flow split is 0.3 for three different flow rates of (14, 28, 56) m^3/hr corresponding to Reynold's number range of (1.6 to 6.6)*10^4. The pressure and velocity fields were analyzed in the whole hydrocyclone with core recirculation. The results are helpful to predict the flow motion inside the cyclone to estimate the oil/water separation process. The present work indicates that the water purity at cyclone exit was 90%, while the obtained oil purity was 38%.

Keywords: CFD, hydrocyclone, oil-water separation, turbulence model.

دراسة عددية لفصل النفط – ماء في هيدروسايكلون احادي المحور

الخلاصة

يعتبر الهايدروسايكلون اداة ممتازة لفصل الماء عن النفط في الموائع المختلطة الخارجة من الابار النفطية. في العمل الحالي تم تقصي الجريان في الهايدروسايكلون المحوري احادي المدخل عدديا باستخدام تقنية ديناميك الموائع الحسابية عن طريق البرنامج الجاهز انسزز- فلونت 19. استخدمت المعادلات ثلاثية الابعاد للاستمرارية والزخم مع نموذج الاضطراب لمحاكاة الجريان القوي الدوامية وامضطرب داخل الهايدروسايكلون. عولج خليط النفط -ماء كمائع ثنائي الطور، واعتبر الماء هو المائع الاساسي والنفط هو المائع الثانوي. اعتمدت النسبة الحجمية للنفط 0.25 وفصل الجريان بـ 0.3 ولمعدل جريان كلي مقداره(14، 28 ، 56م^3/ساعة) والذي يمثل عدد رينولدز مقداره (1.6 الى 6.6 *10^4). تم تحليل الضغط ونطاق السرعة على مدى الهايدروسايكلون مع التدوير الحاصل في القلب. النتائج كانت معبرة عن حركة المائع داخل السايكلون واوضحت عملية فصل النفط عن الماء. تم التوصل الى ان نسبة نقاوة الماء الخارج من الهايدروسايكلون بلغت 90% ، و نقاوة النفط بلغت 38%.

Open Access
No. 34 part 1, March 2022, pp.154-172
P- ISSN: 2220-5381
E- ISSN: 2710-1096

1. Introduction

The hydrocyclone technique is one of the most efficient and proven oil/water separation technology due to its simplicity, compactness, robustness, and low manufacturing and maintenance costs.

First traditional liquid-liquid hydrocyclone separator (LLHC) design was produced by (Dirkzwager, 1996) to study the flow behavior for single phase and two phase flow in axial cyclone [1]. A numerical model for liquid-liquid turbulent flow called (HAAS) is predicted by [2], its showed that the HAAS model is very time efficient in cyclone design, The design of (LLHC) is further investigated using two commercial CFD package and compared it with the experimental results, It was found that the main features of the flow were qualitatively well represented in the numerical simulations, however large quantitative difference were found between the numerical results and experimental data [3]. The swirl number at any location along the pipe length depends on the swirl number at inlet, Reynolds number, the distance from the pipe inlet, the pipe diameter and the nature of the inlet swirl as found by [4]. Laser Doppler anemometry (LDA) is used to measure and compare the tangential and axial mean velocity components in the cyclone with numerical results by [5]. The sensitivity of flow field and cyclone efficiency with the variation of the swirl vanes geometry is shown experimentally by [6]. The fluid flow in cyclone inserted with different guide vane designs is predicted by [7]. It is compared with that predicted in conventional cyclone. These vanes consist of three semicircle plates, each plate form 30^{o} with the pipe axis. The flow field through this pipe was measured by PIV (Particle Image Velocimetry). The results show that the flow pattern inside the current cyclone is improve where its compare with traditional design, also the experimental results predicted that the velocity field is influence by the inlet floe rate and low sensitive to the flow split when its ration less than 13%. One phase laminar flow in axial hydrocyclone is investigated numerically and experimentally to show the flow features and pressure drop under swirl flow condition [8]. Based on the numerical approach the literature survey showed that we can get more details about the feature of the swirl flow in vane type cyclone and the effect of design parameters. An increase in swirl strength is obtained with the increase in the vane deflection angle, number of vanes, inlet flow rate, then an increase in the

Open Access
No. 34 part 1, March 2022, pp.154-172
P- ISSN: 2220-5381
E- ISSN: 2710-1096

separation efficiency is reports as stated by [9] and [10]. The effect of replacing the cylindrical pipe by the conical pipe cyclone is studied by [11]. This Causes a reduction in the recirculation zone and improve the separation efficiency by rises the tangential and axial velocity components. This is considered a worth improvement in the cyclone specifications. The separation of oil/water mixture by filtering hydrocyclone (a porous ceramic membrane) is studied numerically and compared with the conventional cyclone by [12]. Eulerian–Eulerian approach and the turbulence model are applied in this study. Velocity, pressure drop and separation performance of the hydrocyclone were analyzed. The results showed that due to the effect of porous wall the oil phase was instable in the cyclone core. The oil concentration and pressure are lower inside the filtering hydrocyclone compared with conventional cyclone. Also the separation efficiency by using porous wall are reduction by about 5%. An axial inlet hydrocyclone with two stages of separator and two light phase outlets is designed by [13]. The effect of the flow rate, oil volume fraction and the split ratio on the predicted cyclone was investigated for water flow rate of (4–7 m^3/h), and oil fraction (1%–10%). The results show that the split ratio affected the separation efficiency. Also the experimental results appeared that the predicted design is suitable for less than 10% oil fraction, and its structure required optimization to extend its application. The effect of the swirl structure parameters on the velocity field for single phase flow is studied numerically by [14]. The results show that the separator parameters (vane outlet and twist angles as well as number of vanes) have proportional effect on the swirling flow inside hydrocyclone., The tangential velocity is improved and then the separation process. A numerical investigation of flow behavior inside axial flow hydrocyclone is conducted by [15]. The aim of this work is to present the structural cyclone effect on the pressure drop and velocity field using mixture multiphase model and Reynolds stress turbulence model. Three different cyclone structures are used, each contains two swirl generators with two light phase outlets. The test chamber for the first cyclone is a conventional cylindrical tube, second cyclone is a conical diffuser tube and that for the last is a multiple stages of contraction. Results showed that the third cyclone structure have a higher pressure drop compared to the second cyclone, and these two cyclones are more efficient than conventional cylindrical cyclone tube.

Open Access
No. 34 part 1, March 2022, pp.154-172
P- ISSN: 2220-5381
E- ISSN: 2710-1096

Despite of understanding the flow field development inside hydrocyclone very limited previous studies treated with oil-water separation for Iraqi specifications in hydrocyclone are found. The small differences in the density between the two fluids required high cyclone design to enhance separation efficiency. The present work concerned with the detection of the flow behavior inside inline axial hydrocyclone that can be used for downhole oil-water separation. Numerical simulation for turbulent swirling flow of oil/water in concurrent axial inlet hydrocyclone is adopted. The purpose of this simulation is to display the flow field inside the hydrocyclone to improve its design parameters under different flow rates and specify the rise in its' performance.

2. Computational model

The concurrent axial inlet hydrocyclone adopted in this work is shown in Figure (1) with the detailed dimensions given in table (1). It mainly consists of cylindrical inlet section, guide vanes separator, cylindrical tube, central oil discharge tube and annular water outlet. A stationary internal swirl element (separator) used in the present study is surrounded by 9 vanes placed within a pipe as presented in Figure (2). This separator consists of a central body of 80mm diameter and 80 mm height which is equipped with vanes that deflect the flow.

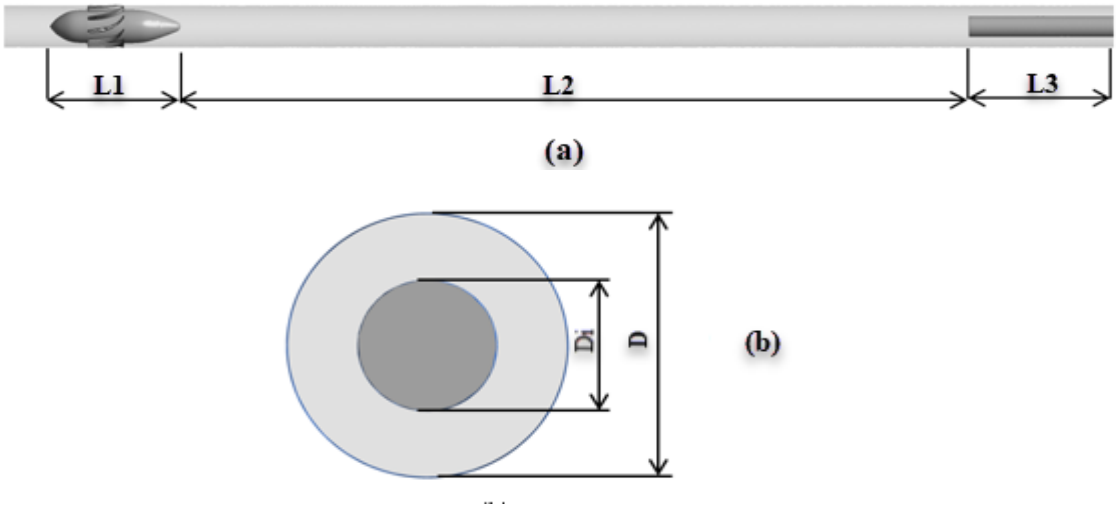

Fig (1): Computational domain of concurrent axial inlet hydrocyclone, a) axial view, b) outlet section.

Open Access
No. 34 part 1, March 2022, pp.154-172
P- ISSN: 2220-5381
E- ISSN: 2710-1096

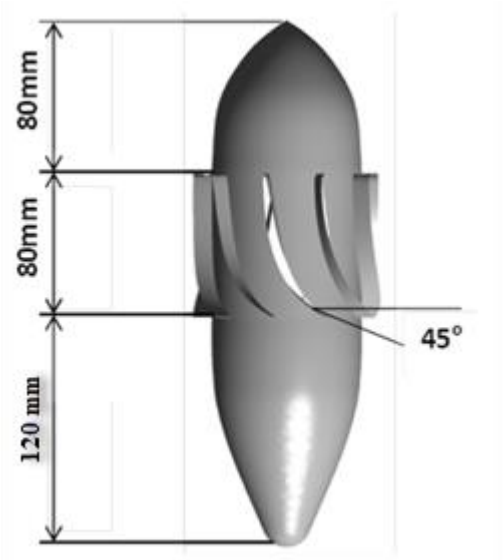

Fig. (2): Separator integrated with vanes.

Table (1): Geometrical dimensions of the concurrent axial inlet hydrocyclone.

L1 (mm)	L2 (mm)	L3 (mm)	D (mm)	Di (mm)
280	1700	300	100	50

3. Mathematical model

The flow behavior inside the cyclone is investigated by the fundamental principles of classical fluid mechanics expressing the conservation of mass and momentum. The continuity and momentum equations for turbulent, isothermal, incompressible flow are: [16]

Continuity equation for phase q

$$\frac{\partial}{\partial t}(\alpha_q \rho_q) + \nabla \cdot (\alpha_q \rho_q \vec{u}_q) = 0 \qquad (1)$$

The momentum equation

$$\rho_q \alpha_q \left(\frac{\partial \vec{u}_q}{\partial t} + \vec{u}_q (\vec{u}_q . \nabla) \right) = -\alpha_q \nabla P + \nabla \cdot (\alpha_q \sigma) + \alpha_q \rho_q g + \rho_q \nabla . (\alpha_q \langle \bar{u}_q \bar{u}_q \rangle) + R_{pq} \qquad (2)$$

Open Access
No. 34 part 1, March 2022, pp.154-172
P- ISSN: 2220-5381
E- ISSN: 2710-1096

where:

P is the pressure shared by all phases.

α_q is the volume fraction of phase q.

$\vec{u}_q$ is the mean velocity.

σ is the viscous stress tensor given by:

$$\sigma = \mu_q(\nabla\vec{u}_q + (\nabla\vec{u}_q)^T$$

$\bar{u}^T$ is the turbulent velocity fluctuation.

R_{pq} is the interface force, this force depends on the friction, pressure, cohesion, and other effects, and is subject to the conditions:

$$\vec{R}_{pq} = -\vec{R}_{qp} \quad (3)$$

and $\vec{R}_{qq} = 0$ (4)

This force defined as :

$$\sum_{p=1}^{n} \vec{R}_{pq} = \sum_{p=1}^{n} K_{pq}(\vec{u}_p - \vec{u}_q) \quad (5)$$

where K_{pq} = (K_{qp}) is the interphase momentum exchange coefficient.

Momentum transfer between the phases is depend on the value of the fluid-fluid exchange coefficient K_{pq}. For liquid-liquid mixture the exchange coefficient K_{pq} is indicated to how the secondary phase (droplet or bubble) do affect the predominant fluid. It can be defined as following:

$$K_{pq} = \frac{\alpha_q \alpha_p \rho_p f}{\tau_p} \quad (6)$$

where

f is the drag function.

τ_p, the particulate relaxation time and is defined as:

$$\tau_p = \frac{\rho_p d_p^2}{18\,\mu_q} \quad (7)$$

d_p is the diameter of the bubbles or droplets of phase p.

Open Access
No. 34 part 1, March 2022, pp.154-172
P- ISSN: 2220-5381
E- ISSN: 2710-1096

Nearly all definitions of (*f*) include a drag coefficient (C_D) that is based on the relative Reynolds number (*Re*). For the model of [17]:

$$f = \frac{C_D Re}{24} \tag{8}$$

C_D =0.44 for Re number up to 1000

Here Re is the Reynolds number based on the relative velocity:

$$Re = \frac{\rho_q |\vec{u}_p - \vec{u}_q| d_p}{\mu_q} \tag{9}$$

The turbulence model (Shear Stress Transport) SST k-omega is used since it has low computational cost and took low iteration time compared to its sensitivity to the complex flow field inside the cyclone. The turbulence governing differential equations are [18] and [19]:

Turbulence Kinetic Energy k

$$\frac{\partial k}{\partial t} + U_j \frac{\partial k}{\partial x_j} = \tau_{ij} \frac{\partial u_i}{\partial x_j} - \beta^* \rho \omega k + \frac{\partial}{\partial x_j}\left[(\mu + \sigma_k \mu_t)\frac{\partial k}{\partial x_j}\right] \tag{10}$$

Specific Dissipation Rate

$$\rho \frac{\partial \omega}{\partial t} + \rho U_j \frac{\partial \omega}{\partial x_j} =$$

$$\frac{\gamma}{v_t}\tau_{ij}\frac{\partial u_i}{\partial x_j} - \beta \rho \omega^2 + \frac{\partial}{\partial x_j}\left[(\mu + \sigma_\omega \mu_t)\frac{\partial \omega}{\partial x_j}\right] + 2\rho(1 - F_1)\sigma_{\omega_2}\frac{1}{\omega}\frac{\partial k}{\partial x_j}\frac{\partial \omega}{\partial x_j} \tag{11}$$

F_1 is blending Function:

$$F_1 = \tanh(arg_1^4)$$

$$arg_1 = min\left[max\left(\frac{\sqrt{k}}{0.09\omega y}, \frac{500v}{y^2\omega}\right), \frac{4\rho\sigma_{\omega 2}k}{CD_{k\omega}y^2}\right] \tag{12}$$

where y is the distance to the next surface and $CD_{k\omega}$ is the positive portion of the cross-diffusion term:

Open Access
No. 34 part 1, March 2022, pp.154-172
P- ISSN: 2220-5381
E- ISSN: 2710-1096

$$CD_{k\omega} = max\left(2\rho\sigma_{\omega 2}\frac{1}{\omega}\frac{\partial k}{\partial x_j}\frac{\partial \omega}{\partial x_j}, 10^{-10}\right) \quad (13)$$

Kinematic eddy viscosity

$$v_T = \frac{a_1 k}{\max(a_1\omega, \Omega F_2)} \quad (14)$$

where Ω is the absolute value of the vorticity and F_2 is second blending function:

$$F_2 = \tanh\left[\left[\max\left(\frac{2\sqrt{k}}{\beta^*\omega y}, \frac{500v}{y^2\omega}\right)\right]^2\right] \quad (15)$$

The SST constants are:

$$\sigma_{k1} = 0\cdot 85 \;;\quad \sigma_{\omega 1} = 0\cdot 5 \;;\quad \beta_1 = 0\cdot 075 \;;\quad a_1 = 0\cdot 31 \;;\quad \beta^* = 0\cdot 09$$

$$k = 0\cdot 41 \;;\quad \gamma_1 = \frac{\beta_1}{\beta^*} - \sigma_{\omega 1}k^2/\sqrt{\beta^*}$$

3.1. Mesh Generation and Computational Algorithm

A computational mesh is generated with 2.9 million numbers of grids, extra work and care was taken to get a good mesh quality of skewness 0.2. Figure (3) presents the mesh adopted on the surface and on the plane through the axis of the separator. The mesh is refined near wall and on the separator surface in order to capture the flow behavior near the wall. SIMPLE (Semi-Implicit Method for Pressure Linked Equations) algorithm is used for pressure-velocity coupling, Diffusive and convective terms were discretized using a hybrid scheme.

Open Access
No. 34 part 1, March 2022, pp.154-172
P- ISSN: 2220-5381
E- ISSN: 2710-1096

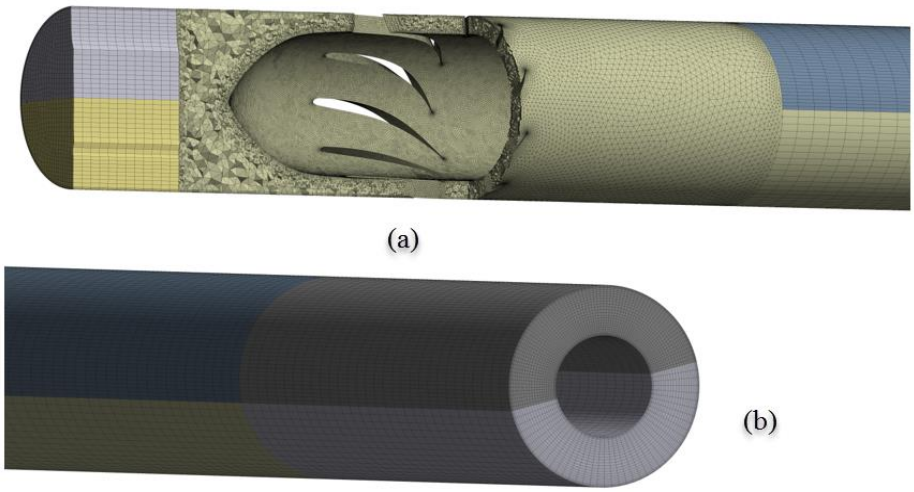

Fig. (3): Mesh generated for hydrocyclone (a) Cross sectional view, (b) Outlet zone.

3.2. Grid independency

Grid independencey is performed in which three different grids are used, coarser mesh 2.7 million elements, medium mesh 2.9 million elements and fine mesh 3 million elements. The tangential velocity distribution at x= 0.5m after separator is presented for these grid systems as shown in Figure (4). It can be shown that the difference in the tangential velocity between the coarser and medium mesh is relatively large, whereas, the difference between medium and fine mesh is less than 3%. Hence the medium system estimate is selected in this work.

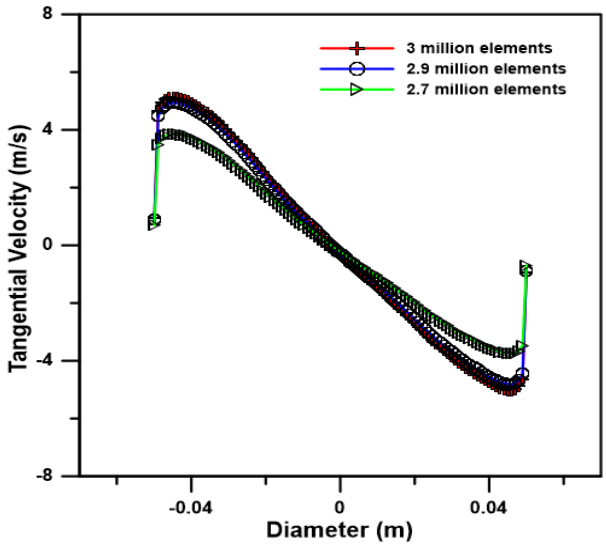

Fig (4): Tangential velocity distribution at different grid numbers of the same model at X = 0.5m.

Open Access
No. 34 part 1, March 2022, pp.154-172
P- ISSN: 2220-5381
E- ISSN: 2710-1096

3.3. Boundary conditions

The computational domain is occupied by two-phase flow. Water corresponds to the continuous phase and the oil represents the dispersed phase within a droplet diameter d_p = 100 µm and volume fraction 0.25. The density and viscosity of water is 1067.8 kg/m^3, 1.183x10^{-3} kg/ms and that for oil is 869 kg/m^3, 8.690x10^{-3} kg/ms, respectively. As a boundary condition, the inlet is defined as a uniform velocity inlet and is taken as 1m/s. The outlets are set to be outflow. No slip boundary conditions are used at solid walls.

4. Results and discussion

4.1. Flow field

Oil/water mixture enters the hydrocyclone with inlet axial velocity of 1 m/s, flow rate of 28 m3/h , oil volume fraction of 0.25 and flow split of 0.3. The fluid flow is analyzed into three velocity components axial (w), radial and tangential velocity (u). The tangential and axial velocity contours inside the cyclone are shown in Figure (5). Tangential velocity is the dominant velocity component in the separator and the key factor which responses for the centrifugal force. It has a direct effect on the separation deteriorate and on the cyclone efficiency. When the tangential velocity increases, the centrifugal force and separation efficiency will increase [20]. The reported values for tangential velocity was 9.93 m/s near the separator middle section while at its nose there were a reverse tangential oil flow. As shown in Figure (6a), the swirl intensity is maximum at the region after separator nose and decays along the axial direction as well as when it approaches the pipe center and pipe wall. Figure (6b) shows the axial flow distribution along the axial hydrocyclone. The axial velocity reaches its peak value in the annular region, this indicated to the favorable forward positive velocity. Its value is rabidly decreases toward the wall, where it falls to zero on the wall (no slip condition). As proceed to the pipe core its rate decline to the negative value, where the unfavorable backward velocity appeared. As fluid flows toward the pipe outlet the axial velocity increases in the core region and reaches to fully developed flow after 1.5m from the separator, at this position the pickup tube is located for oil collection.

Open Access
No. 34 part 1, March 2022, pp.154-172
P- ISSN: 2220-5381
E- ISSN: 2710-1096

The inlet flow rate is considered as the main parameter that affects the separation process. Figure (7a) shows an improve in the axial velocity as flow rate increases. The influence of increasing the inlet flow rate on the swirling intensity increase and then tangential velocity is shown in Figure (7b).

As the flow leaves the separator, the velocity vector shows that the backward flow have maximum value at the pipe core due to the adverse pressure gradient causes a recirculation zone as illustrated in Figure (8). The strong swirl intensity in the region after separator induces the lowest static pressure in this region. A gradual reduction in swirl intensity is figured along the test pipe due to the wall friction effect. The flow reverses its direction after 1m downstream the separator, and near the pipe outlet the flow be stable.

The oil and water streamlines are shown in Figure (9). When the fluid mixture is deflected by the separator vanes it gains a centrifugal force effect due to the difference in the density between the two phases. This results a separation between the phases, in which the heavy fluid (water phase) have a large spin and make it closer to the wall, while the lighter fluid (oil phase) segregate towards the center of the pipe. Downstream of the separator, the fluid particle spin is dampened due to the viscous effects so the tangential velocity component dissipates and the centrifugal field loses its intensity

4.2. Pressure distribution

Figure (10) shows the radial pressure distribution at 0.2m from separator. The large pressure drop in the pipe core indicates the high tangential velocity and increases the cross sectional area in the region after separator. This leads to a large pressure drop near the wall and in the pipe core. The pressure drop mainly affects in generate the recirculation zone and causes the adverse axial velocity. This behavior is clearly appeared in the axial pressure distribution presented in Figure (11) and it is identical with results obtained by [21].

4.3. Oil volume fraction

The distribution of oil volume fraction presented in Figure (12) shows a good separation of phases. A region of pure oil is seen near the separator with volume fraction reaches 63% as a maximum value, and all of the separated oil is oriented to the

Open Access
No. 34 part 1, March 2022, pp.154-172
P- ISSN: 2220-5381
E- ISSN: 2710-1096

pickup tube. Due to the high effect of centrifugal force at the end of separator the oil phase moves inwards and cumulatively presented in the pipe core. Most of this oil captured is by the backflow, so the oil core will return to move out due to instability of the flow in this region. The region of reverse flow has bad effect on the separation process, since most of the oil that is collected in that region recirculated back into the outlet region. So the light phase pick up tube should be located at far away from the separator where the reverse flow be small or ended. It can be seen from Figure (12) that some oil is spill over the pickup tube and flowing towards water outlet. For mixture flow rate of 28 m^3/hr the obtained water purity was 90%, while oil purity was 38% for inlet oil volume fraction of 0.25 with mass flow split of 0.30. Figure (13) shows the radial distribution of the oil volume fraction at x=0.5m after separator for three different flow rates namely (14, 28, 59)m^3/hr . Its observed as the inlet flow rate increases the oil cumulated in the core region increases also, and this leads to enhancement in the separation process.

5. Conclusion

In this work, a numerical investigation of oil-water separation based on inline axial-flow hydrocyclone technique to contribute in recovering oil production and minimize water extra producing. This investigation is mainly attempted to exposure the performance of this oil/water separator for Iraqi oil specifications. The results show that:

1- The swirl intensity and the centrifugal force have highest value at cyclone segment after the separator, then decreases along the cyclone axis. The tangential velocity is directly affected by this force, its profile consist of combination of free and force vortex distributions.
2- The oil vortex is close to the pipe core and its strength decays obviously after half of the pipe.
3- Pressure has a minimum value in the core region after separator and it has a main effect on the adverse axial flow.
4- Water purity at cyclone exit was 90% for 25% oil volume fraction received at its inlet, while the obtained oil purity was 38%.

Open Access
No. 34 part 1, March 2022, pp.154-172
P- ISSN: 2220-5381
E- ISSN: 2710-1096

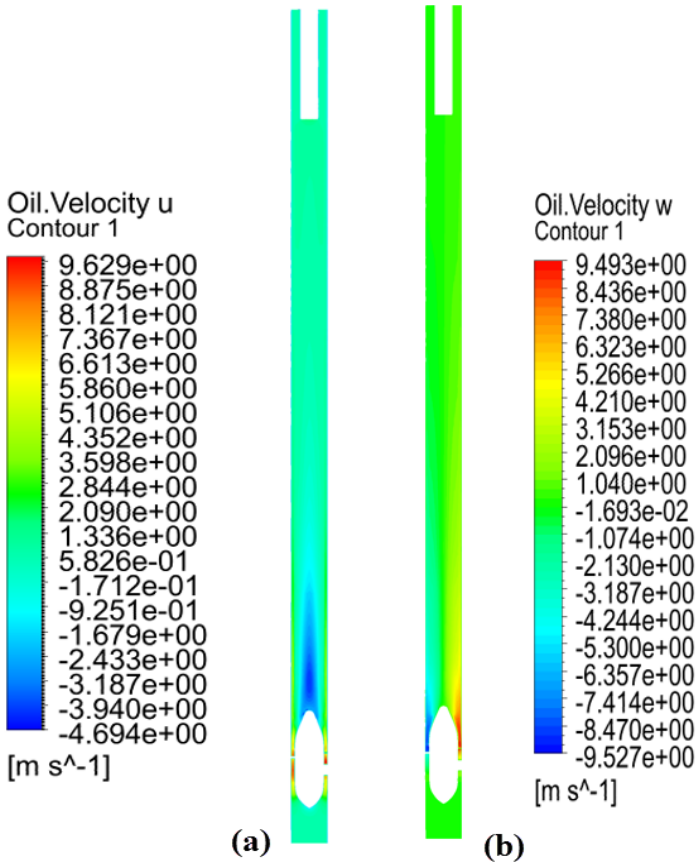

Fig. (5): Velocity contour along the axial direction (a) Tangential velocity u (b) Axial velocity w.

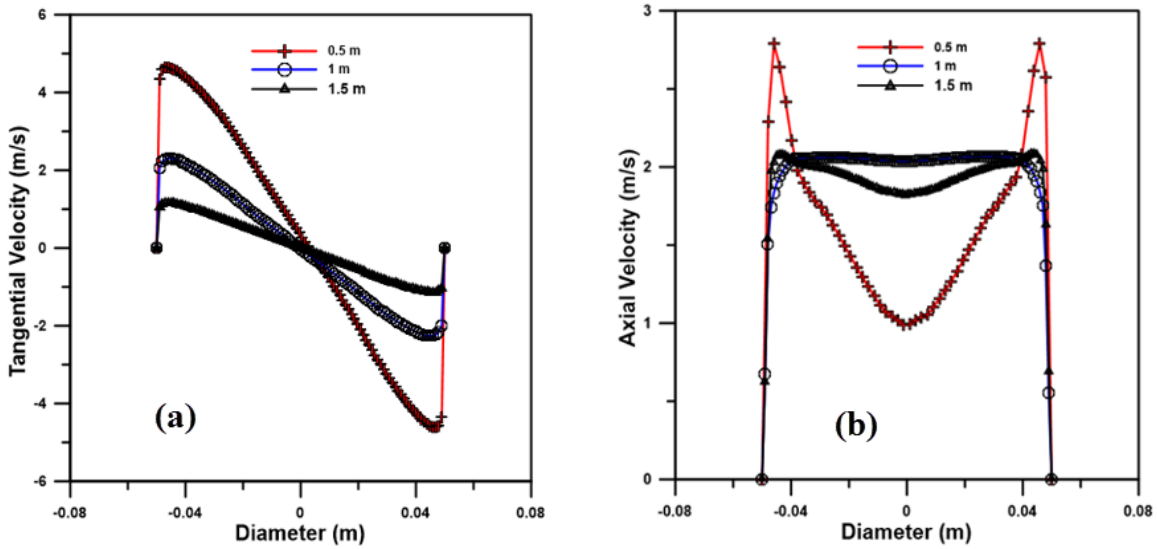

Fig. (6): Velocity distribution at selected position along the pipe a) tangential velocity, b) axial velocity

Open Access
No. 34 part 1, March 2022, pp.154-172
P- ISSN: 2220-5381
E- ISSN: 2710-1096

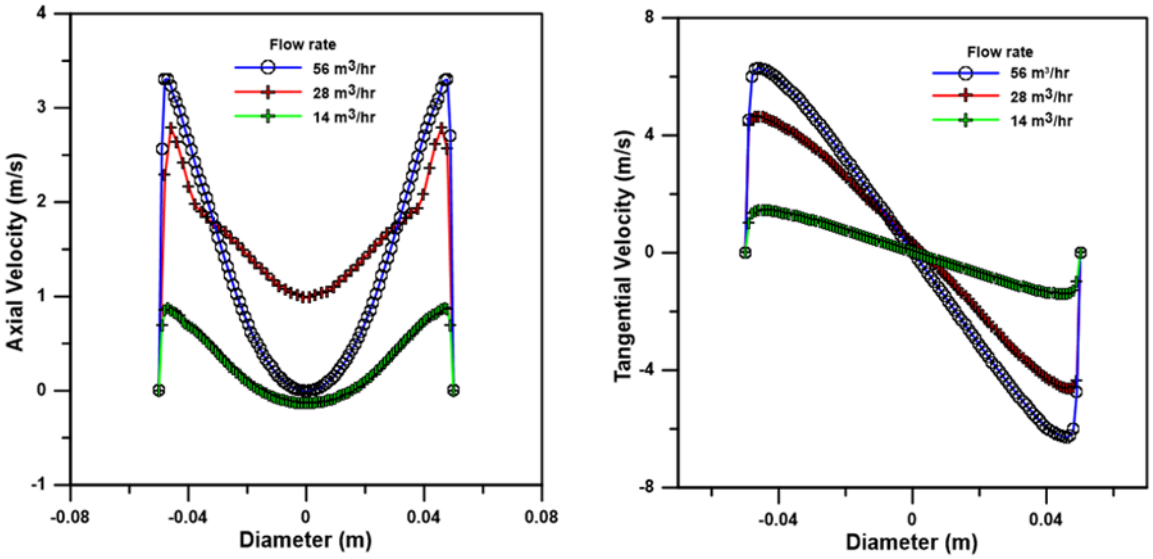

(a) (b)

Fig. (7): Velocity components distribution at x=0.5m for different flow rate (a) Tangential, (b) Axial.

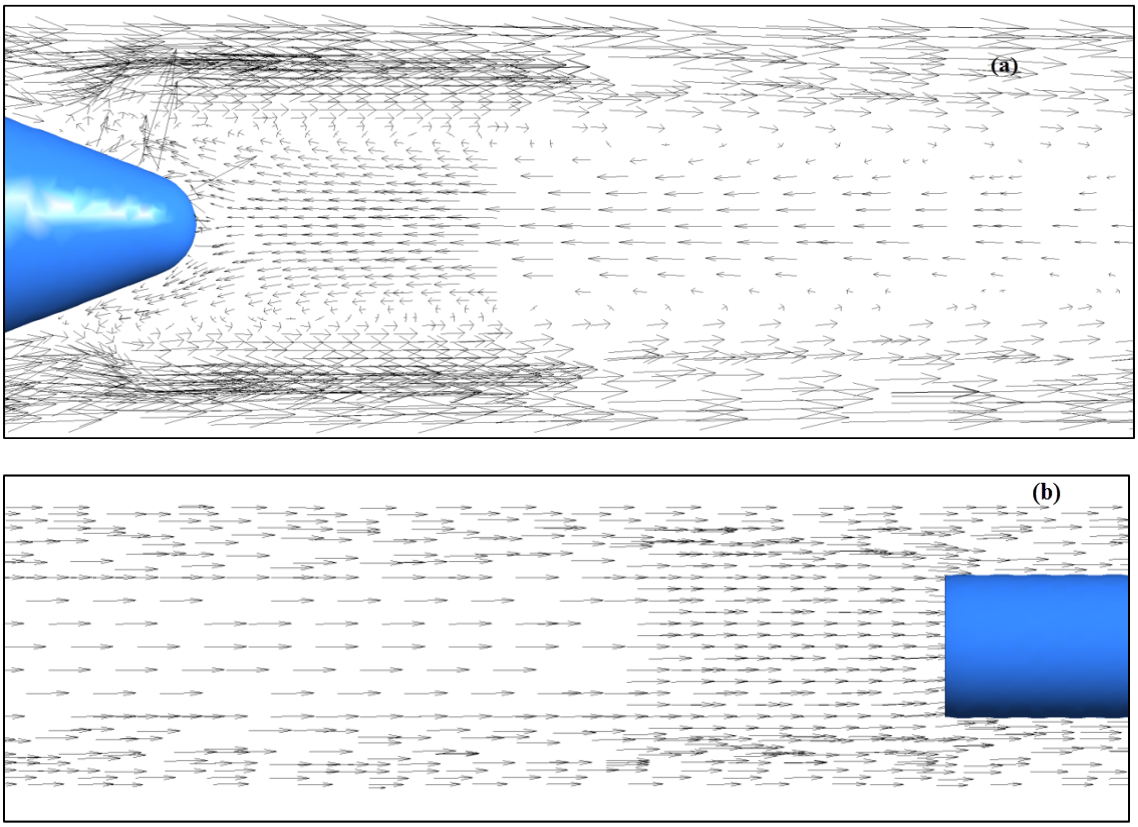

Fig. (8): Velocity vector inside cyclone (a) after separator, (b) upstream the pickup tube.

Open Access
No. 34 part 1, March 2022, pp.154-172
P- ISSN: 2220-5381
E- ISSN: 2710-1096

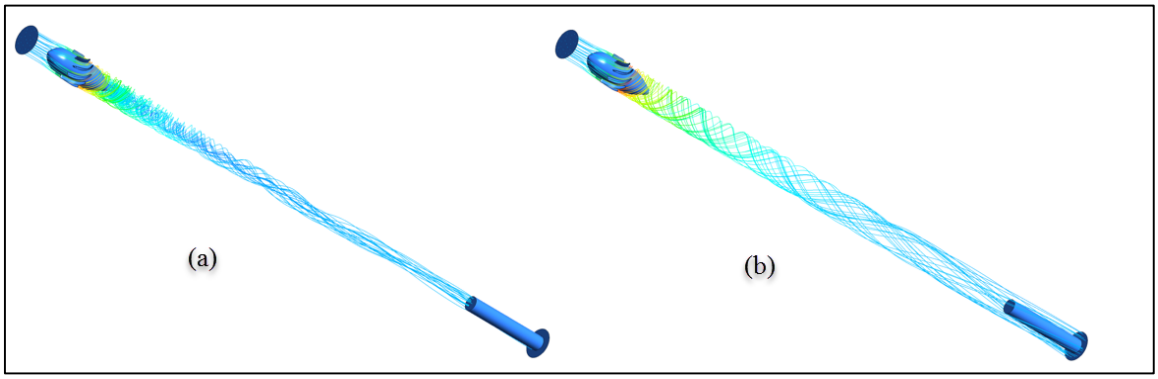

Fig. (9): Stream line for (a) Oil, (b) Water.

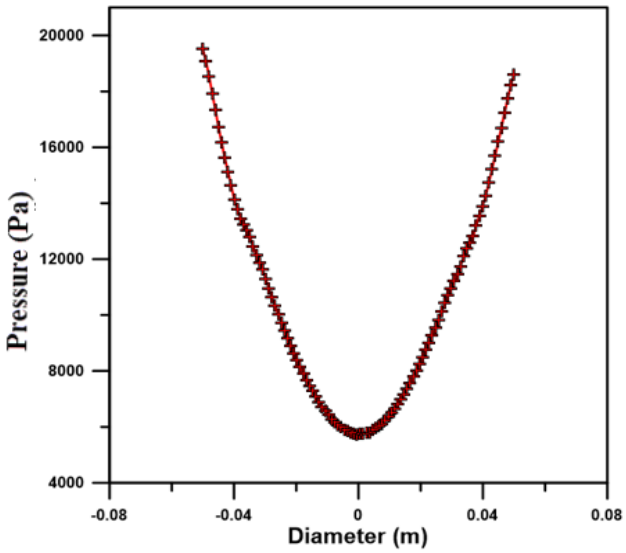

Fig. (10): Radial pressure distribution at 0.2m after separator.

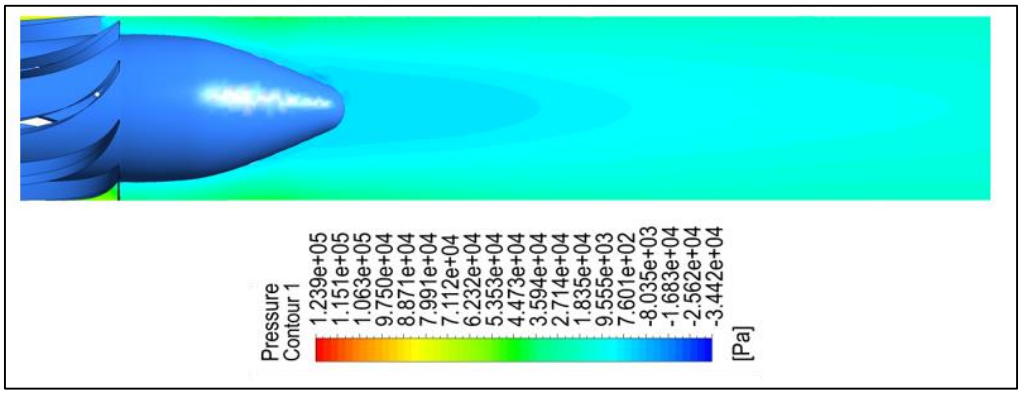

Fig. (11): Contours of the pressure distribution in the region after separator.

Open Access
No. 34 part 1, March 2022, pp.154-172
P- ISSN: 2220-5381
E- ISSN: 2710-1096

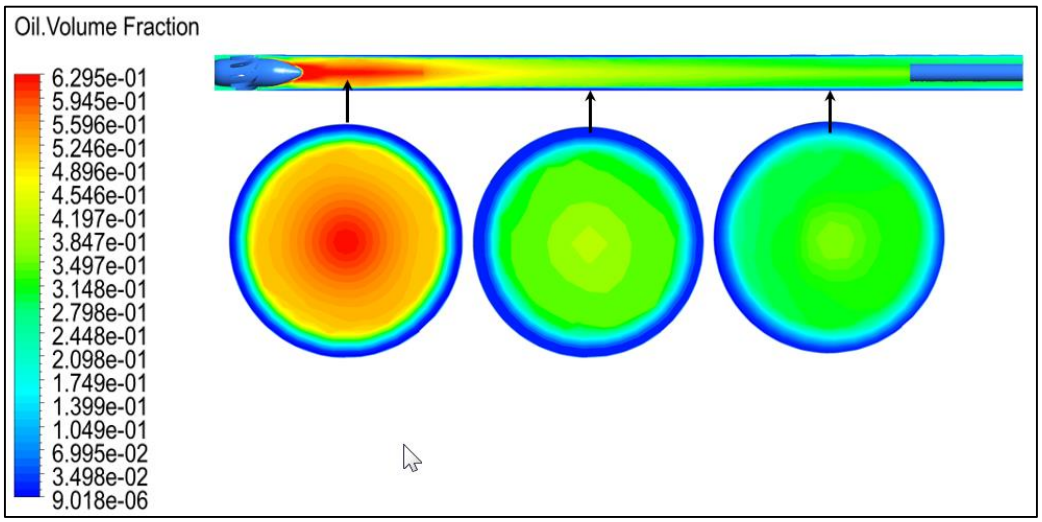

Fig. (12): Oil volume distribution along the hydrocyclone.

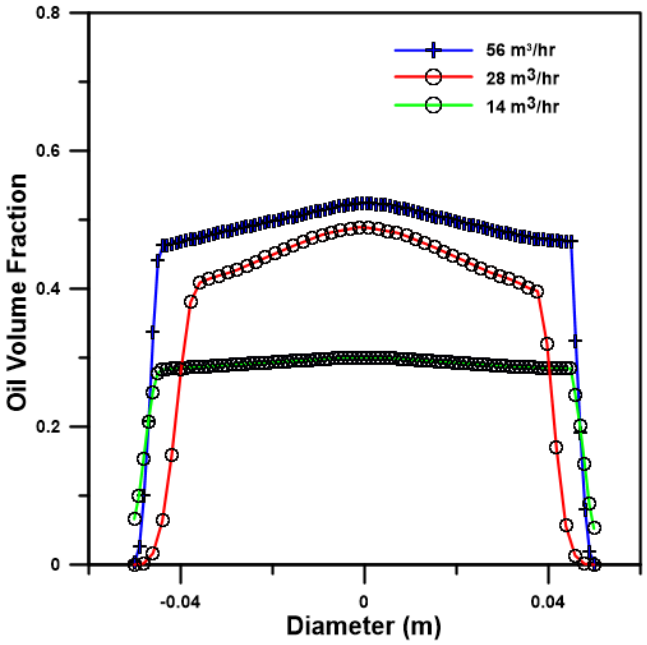

Fig. (13): Oil volume distribution for different flow rate at x=0.5m after separator.

Journal of Petroleum Research and Studies

Open Access
No. 34 part 1, March 2022, pp.154-172

P- ISSN: 2220-5381
E- ISSN: 2710-1096

Nomenclature

Symbol	Description	Symbol	Description
Latin symbol		$\nabla\vec{u}$	turbulent velocity fluctuation (m/s)
C_D	drag coefficient	$\vec{V}$	velocity (m/s)
D	cyclone diameter (mm)	X	Axial direction
Di	Pickup tube diameter (mm)	x_j	coordinate (m)
d_p	droplet diameter (m)	y	distance to the next surface
f	drag function.	**Greek letters**	
F_1	blending Function	α	volume fraction, or Turbulence model constants
F_2	second blending function	β	Turbulence model constants
g	gravitational acceleration (m/s^2)	μ_t	Turbulent eddy viscosity(kg/ms)
k	turbulence Kinetic Energy	μ	dynamic viscosity (kg/m.s)
K_{pq}	interphase momentum exchange coefficient	ν	Kinematic viscosity(m^2/s)
L1	axial separator length (mm)	ω	Specific Dissipation Rate
L2	cyclone Test tube length (mm)	Ω	absolute value of the vorticity
L3	pickup tube length (mm)	ρ_j	density (kg/m^3)
P	pressure (Pa)	σ	Turbulence model constants, or Viscous stress tensor(kg/ms^2)
R	interface force	τ_p	particulate relaxation time
Re	Reynolds number	**Abbreviations**	
U_j	velocity component(m/s)	CFD	Computational Fluid Dynamics
$\vec{u}$	mean velocity (m/s)	SST	Shear Stress Transport

Open Access
No. 34 part 1, March 2022, pp.154-172
P- ISSN: 2220-5381
E- ISSN: 2710-1096

References

[1] M. Dirkzwager, "A New Axial Cyclone Design for Fluid-Fluid Separation," *PhD. thesis, Delft University of Technology: Delft, Netherlands*, 1996.

[2] R. Delfos, S. Murphy, D. Stanbridge, Z. Olujić, and P. Jansens, "A design tool for optimising axial liquid–liquid hydrocyclones," Minerals Engineering, vol. 17, no. 5, pp.721–731, 2004.

[3] S. Murphy, R. Delfos, M. Pourquie, Z. Olujić, P. Jansens, and F. Nieuwstadt, "Prediction of strongly swirling flow within an axial hydrocyclone using two commercial CFD codes," Chemical Engineering Science, vol. 62, no. 6, pp.1619–1635, 2007.

[4] F. Ayinde, "A generalized relationship for swirl decay in laminar pipe flow," Sadhana, vol. 35, no. 2, pp.129–137, 2010.

[5] L. Van Campen, R. Mudde, J. Slot, and H. Hoeijmakers, "A numerical and experimental survey of a liquid-liquid axial cyclone," International Journal of Chemical Reactor Engineering, vol. 10, no.1, 2012.

[6] Y. Zhang, Y. Wang, Y. Zhang, L. Zhao, F. Li, F. Wang, and G. Zheng, "Design of Hydrocyclone With Axial Inlet and its Performance Used in Wellbore," ASME 2014 33rd International Conference on Ocean, Offshore and Arctic Engineering.

[7] S. Shi, and J. Xu, "Flow field of continuous phase in a vane-type pipe oil–water separator," Experimental Thermal and Fluid Science, vol. 60, pp.208–212, 2015.

[8] A. Rocha, A. Bannwart, and M. Ganzarolli, "Numerical and experimental study of an axially induced swirling pipe flow," International Journal of Heat and Fluid Flow, vpl. 53, pp. 81–90, 2015.

[9] A. Rocha, A. Bannwart, and M. Ganzarolli, "Effects of inlet boundary conditions in an axial hydrocyclone. Journal of the Brazilian Society of Mechanical Sciences and Engineering, vol. 39, no. 9, pp. 3425–3437, 2017.

[10] Y. Fan, L. Ailan, G. Xueyan, "Numerical Simulation on the Performance of Axial Vane Type Gas-Liquid Separator with Different Guide Vane Structure," International Journal of Fluid Machinery and Systems, vol. 10 no.1, pp.86–98, (2017).

[11] J. Hamza, H. Al-Kayiem, and T. Lemma, "Experimental investigation of the separation performance of oil/water mixture by compact conical axial hydrocyclone" Thermal Science and Engineering Progress, vol. 17, 100358, 2020.

Open Access
No. 34 part 1, March 2022, pp.154-172
P- ISSN: 2220-5381
E- ISSN: 2710-1096

[12] S. Nunes, H. Magalhães, S. Neto, A. Lima, L. Nascimento, F. Farias, and E. Lima, "Impact of permeable membrane on the hydrocyclone separation performance for oily water treatment," Membranes, vol. 10, no. 11, pp.1–21, 2020 .

[13] M. Zhan, X. Cheng, W. Yang, F. Zhang, P. Guo, and Q. Shen, "Numerical investigation on the swirler parameters for an axial liquid-liquid hydrocyclone," IOP Conference Series: Earth and Environmental Science, 675(1), 2021.

[14] M. Zhan, W. Yang, F. Zhang, C. Luo, H. Wu, P. Guo, Q. Shen, X. Zeng, and C. Yan, "Experimental Investigation on the Separation Performance for a New Oil-Water Separator," Frontiers in Energy Research, 8(February), Article 608586, 2021.

[15] X. Zeng, Y. Xu, L. Zhao, G. Fan, and C. Yan, "Numerical investigation on axial liquid-liquid separators with different swirl chambers," Chemical Engineering and Processing - Process Intensification, 161(February), 108324, 2021.

[16] FLUENT 6.3 User's Guide, September 2006

[17] L. Schiller, and A. Naumann, “About the basic calculations in gravity processing," Journal of the Association of German Engineers, vol.77, no. 318, 1933. In German.

[18] D. Wilcox, "Reassessment of the Scale-Determining Equation for Advanced Turbulence Models," AIAA Journal, vol. 26, no. 11, pp. 1299-1310, 1988.

[19] F. Menter, "Two-Equation Eddy-Viscosity Turbulence Models for Engineering Applications," AIAA Journal, vol.32, no.8, pp. 1598-1605, 1994.

[20] K. Bhaskar, Y. Murthy, M. Raju, S. Tiwari, J. Srivastava, and N. Ramakrishnan, "CFD simulation and experimental validation studies on hydrocyclone," Minerals Engineering, vol. 20, no. 1, pp. 60–71, 2007.

[21] M. Jiang, and L. Zhao, "Pressure and separation performance of oil/water hydrocyclones," Production and Operations Symposium, 2007.